materials

MDPI

Article

Phase Stability and Mechanical Properties of Al_8Fe_4RE via First-Principle Calculations

Rongcheng Wang [1,2], Xiaoma Tao [2], Hongmei Chen [2] and Yifang Ouyang [1,2,*]

[1] School of Materials Science and Engineering, South China University of Technology, Guangzhou 510640, China; rong_phy@163.com

[2] Guangxi Key Laboratory of Processing for Non-ferrous Metallic and Featured Materials, School of Physical Science and Technology, Guangxi University, Nanning 530004, China; taoxiaoma@gxu.edu.cn (X.T.); chenhm@gxu.edu.cn (H.C.)

* Correspondence: ouyangyf@gxu.edu.cn

Received: 12 February 2019; Accepted: 25 February 2019; Published: 27 February 2019

Abstract: We report on the phase stability, elastic, electronic, and lattice dynamic properties of 17 Al_8Fe_4RE (RE = Sc, Y, La–Lu) intermetallic compounds (IMCs) using first-principle calculations. The calculated lattice constants coincided with the experimental results. The calculated enthalpy formation indicated that all the 17 IMCs are stable. The elastic constants and various moduli indicated that Al_8Fe_4RE can be used as a strengthening phase due to its high Young's modulus and shear modulus. The 3D surfaces of Young's modulus for Al_8Fe_4RE showed anisotropic behavior, and the values of hardness for the IMCs were high (about 14 GPa). The phonon spectra showed that only Al_8Fe_4Y had a soft mode, which means the other IMCs are all dynamically stable.

Keywords: first-principle calculation; Al_8Fe_4RE; elastic properties; lattice dynamic

1. Introduction

Due to their low density, low thermal conductivity, relative high strength, and low material cost, Al–Fe-based alloys have been studied extensively over the last few decades [1–4]. Al–Fe-based alloys are promising, high-temperature structural materials; however, their limited ductility at room temperature and the reduction in strength above 600 °C obstruct their application as high-temperature structural materials. Nevertheless, some recent investigations have shown that the mechanical properties can be effectively improved by controlling the microstructure, composition, and alloying elements [5–8].

As we known, rare-earth (RE) elements are special modifiers that are commonly used in Al-based and Fe-based alloys. Thus, the addition of RE elements in Al–Fe-based alloys may affect the microstructure and improve the mechanical properties of these alloys. When RE elements are added, Al–Fe–RE intermetallic compounds (IMCs) form, which affects the phase relationship and microstructure of Al–Fe-based alloys. The mechanical properties of Al–Fe-based alloys are consequently improved due to the changes in composition and microstructure. In previous works, Al–Fe–RE (RE = Y, Ce, Nd, Gd, Er) ternary phase diagrams have been experimentally investigated [9–13], and the ternary IMCs have been determined. The Al_8Fe_4RE IMCs are observed at the Al-rich corner, and they have a tetragonal crystal structure. The 17 Al_8Fe_4RE (RE = Sc, Y, La, Ce, Nd, Eu–Er, and Lu) IMCs have also been previously determined in experiments [14–25]. Using the empirical electron theory (EET), Al_8Fe_4Ce was found to be favorable for the stability of the Al-based alloy as a strengthening phase [15]. The magnetic properties of Al_8Fe_4RE have also been investigated [16–21], and the electronic conductivity [22] and the negative magnetoresistivity [23] of Al_8Fe_4RE have also been studied. Using the lattice inversion method, the lattice constants and

lattice vibration spectra of Al_8Fe_4RE (RE = Sc, Ce, Nd, Sm) have been reported [24,25]. As a potential strengthening phase and as magnetic materials, the structural stability and electronic and elastic properties of Al_8Fe_4RE are very important for material design and for further development. However, few studies have focused on the electronic and elastic properties of Al_8Fe_4RE IMCs. Thus, the aim of this work was to study the physical properties of 17 Al_8Fe_4RE (RE = Sc, Y, and La–Lu) IMCs using first-principle (FP) calculations.

2. Computational Details

The FP calculations were performed with the VASP code [26,27] using the projector augmented wave (PAW) method [28,29] and the generalized gradient approximation (GGA) [30]. The GGA-PBE (Generalized Gradient Approximation-Perdew–Burke–Ernzerhof) potentials of Al, Fe, Sc, Y_sv, La_s, Yb_2, and RE_3 (others) were used in this work. The FP calculations were performed with cutoff energy of 500 eV, Monkhorst–Pack K-point meshes [31], and a 0.05 eV smearing parameter with the Methfessel–Paxton technique [32].

The formation enthalpy and cohesive energy of the Al_8Fe_4RE alloys can be estimated from the following equations:

$$\Delta H(Al_8Fe_4RE) = E(Al_8Fe_4RE) - 8E(Al) - 4E(Fe) - E(RE) \quad (1)$$

$$E_c(Al_8Fe_4RE) = E(Al_8Fe_4RE) - 8E_{single}(Al) - 4E_{single}(Fe) - E_{single}(RE) \quad (2)$$

where $E(Al_8Fe_4RE)$, $E(Al)$, $E(Fe)$, and $E(RE)$ are the equilibrium first-principles-calculated total energies of the Al_8Fe_4RE IMCs, Al, Fe, and rare earth element, respectively. In the calculation, the Al, Ce, and Yb have the face-centered cubic (FCC) structure, Fe and Eu have the body-centered cubic (BCC) structure, and the others have the hexagonal close packed (HCP) structure. The $E_{single}(Al)$, $E_{single}(Fe)$, and $E_{single}(RE)$ are the total energies of the isolated atoms.

For a tetragonal structure, there are six independent single-crystal elastic constants: C_{11}, C_{12}, C_{33}, C_{13}, C_{44}, and C_{66}. The calculated details can be found in [33] and are not recalled here. The effective elastic moduli can be estimated with Voigt [34], Reuss [35], and Hill [36] methods. Usually, the Voigt–Reuss–Hill (VRH) value is used as an effective data [37].

3. Results and Discussion

3.1. Phase Stability

The lattice constants, formation enthalpies, cohesive energies of 17 Al_8Fe_4RE IMCs were calculated, and the obtained results are listed in Table 1 with experimental [14] and theoretical data [38]. It can be seen from Table 1 that the calculated lattice constants of Al_8Fe_4RE IMCs were all in coincident with the experimental data [14], and the lattice constants slightly reduced with the increase in atomic number, which is known as the "lanthanide contraction". This phenomenon occurs in RE pure elements and RE-bearing IMCs [39–41]. The formation enthalpies (ΔH) and cohesive energies (E_c) of Al_8Fe_4RE IMCs were all negative, showing that all the Al_8Fe_4RE IMCs are stable. For Al_8Fe_4Gd, the formation energy of CALPHAD is -0.6114 eV/atom [38], and the calculated result was -0.4254 eV/atom. As we known, the CALPHAD data is estimated from some experimental phase and thermodynamic data, which is the reason for the difference in the two results. However, some further experiments are needed to validate the calculated ΔH and E_c of Al_8Fe_4RE. The magnetic moments of Al_8Fe_4RE were also obtained. The magnetic moments changed from 1.4 to 1.6 μ_B per Fe atom. Here, it should be noted that the RE_3 with f-electrons were kept frozen in core used in the present work.

Table 1. Lattice constants, formation enthalpy, cohesive energy, and magnetic moments of Al_8Fe_4RE IMCs.

Phases	Lattice Constants		△*H* (eV/atom)	*Ec* (eV/atom)	Magnetic (μ_B/Fe)	Ref.
	a (Å)	*c* (Å)				
Al_8Fe_4Sc	8.597	5.001	−0.4238	−4.5211	1.426	Present
	8.70	4.81				[14]
Al_8Fe_4Y	8.696	5.024	−0.4322	−4.5221	1.500	Present
	8.750	5.060				[14]
Al_8Fe_4La	8.849	5.045	−0.3843	−4.4922	1.602	Present
	8.900	5.075				[14]
Al_8Fe_4Ce	8.829	5.046	−0.3843	−4.4963	1.599	Present
	8.793	5.047				[14]
Al_8Fe_4Pr	8.802	5.042	−0.3955	−4.5076	1.584	Present
	8.824	5.054				
Al_8Fe_4Nd	8.781	5.039	−0.4043	−4.5152	1.571	Present
	8.804	5.054				[14,24]
	8.875	5.211				
Al_8Fe_4Pm	8.762	5.035	−0.4122	−4.5173	1.559	Present
Al_8Fe_4Sm	8.748	5.032	−0.4162	−4.5223	1.549	Present
	8.770	5.053				[14,24]
	8.863	5.188				
Al_8Fe_4Eu	8.732	5.035	−0.4328	−4.5259	1.536	Present
	8.784	5.051				[14]
Al_8Fe_4Gd	8.719	5.028	−0.4254	−4.5283	1.524	Present
	8.743	5.052	−0.6114			[14,38]
Al_8Fe_4Tb	8.708	5.024	−0.4277	−4.5283	1.511	Present
	8.740	5.036				[14]
Al_8Fe_4Dy	8.697	5.022	−0.4291	−4.5275	1.499	Present
	8.728	5.050				[14]
Al_8Fe_4Ho	8.688	5.021	−0.4298	−4.5262	1.488	Present
	8.720	5.038				[14]
Al_8Fe_4Er	8.678	5.018	−0.4296	−4.5247	1.477	Present
	8.700	5.028				[14]
Al_8Fe_4Tm	8.669	5.016	−0.4288	−4.5224	1.466	Present
	8.688	5.037				[14]
Al_8Fe_4Yb	8.703	5.049	−0.3652	−4.2378	1.559	Present
	8.691	5.017				[14]
Al_8Fe_4Lu	8.653	5.012	−0.4256	−4.5174	1.450	Present
	8.687	5.030				[14]

3.2. Mechanical Properties

In order to shed some light on the mechanical properties of Al_8Fe_4RE IMCs, the elastic constants (C_{ij}) of Al_8Fe_4RE IMCs were calculated, and the results are listed in Table 2.

Obviously, the present elastic constants C_{ij} of the 17 Al_8Fe_4RE IMCs met the requirement of stability conditions with $C_{11} > 0$, $C_{33} > 0$, $C_{44} > 0$, $C_{66} > 0$, $(C_{11} - C_{12}) > 0$, $(C_{11} + C_{33} - 2C_{13}) > 0$, and $[2(C_{11} + C_{12}) + C_{33} + 4C_{13}] > 0$. For Al_8Fe_4RE (RE = Sc, La, Ce, Pr, Yb), $C_{11} < C_{33}$ indicated that the bonding strength along the [100] and [010] directions was softer than that along the [001] direction. However, for the others, $C11 > C33$, the opposite tendency occurred. $C44 < C66$ meant the [100](001) shear was easier than the [100](010) shear for the 17 Al_8Fe_4RE IMCs.

The bulk modulus (B), shear modulus (G), Young's modulus (E), and Poisson's ratio (σ) of the 17 Al_8Fe_4RE IMCs were estimated, and the results are listed in Table 3. The bulk moduli (B) of the 17 Al_8Fe_4RE IMCs were larger than that of Al (72 GPa) [42], and the shear moduli (G) and Young's moduli (E) of the 17 Al_8Fe_4RE IMCs were three times that of Al (27 GPa and 71 GPa) [42]. In order to compare them clearly, the arithmetic average values of pure Al, Fe, and RE with the weight of composition were calculated for Al_8Fe_4RE IMCs, and the results are shown in Figure 1. Obviously, the presently calculated bulk moduli (B) were 1.2 times than that of the arithmetic average values, and

the presently calculated G and E were close to two times the arithmetic average values. This indicates that the Al_8Fe_4RE IMCs may be used as a strengthening phase.

Table 2. The calculated elastic constants of Al_8Fe_4RE intermetallic compounds (IMCs) (unit in GPa).

Phases	C_{11}	C_{12}	C_{13}	C_{33}	C_{44}	C_{66}
Al_8Fe_4Sc	266.15	49.09	53.62	268.07	68.43	76.57
Al_8Fe_4Y	264.94	46.05	52.36	259.71	70.02	77.63
Al_8Fe_4La	254.17	41.90	52.25	262.29	67.73	70.86
Al_8Fe_4Ce	252.33	42.85	51.22	255.08	68.08	71.60
Al_8Fe_4Pr	255.29	43.90	51.40	255.34	68.35	71.43
Al_8Fe_4Nd	257.70	44.72	51.42	256.22	68.77	71.96
Al_8Fe_4Pm	260.29	45.46	51.61	257.71	69.33	73.14
Al_8Fe_4Sm	261.44	45.87	51.76	258.24	69.50	73.91
Al_8Fe_4Eu	262.97	46.12	51.84	258.83	69.74	74.79
Al_8Fe_4Gd	263.60	46.01	51.87	258.92	69.75	76.04
Al_8Fe_4Tb	264.58	46.22	52.25	259.89	69.80	76.95
Al_8Fe_4Dy	265.29	46.15	52.38	260.28	70.09	77.59
Al_8Fe_4Ho	265.91	46.22	52.78	261.12	70.39	78.01
Al_8Fe_4Er	266.61	46.29	53.14	261.95	70.74	78.24
Al_8Fe_4Tm	267.35	46.46	53.64	262.82	70.90	77.65
Al_8Fe_4Yb	247.62	38.03	48.66	249.15	64.34	66.59
Al_8Fe_4Lu	254.53	44.55	51.63	250.65	67.35	73.88

Table 3. The calculated bulk modulus B, shear modulus G, Young's modulus E, Poisson's ratio v, B/G ratio, and hardness H of Al_8Fe_4RE IMCs.

Phases	B (GPa)	G (GPa)	E (GPa)	v	B/G	H
Al_8Fe_4Sc	123.66	83.85	205.17	0.224	1.475	13.94
Al_8Fe_4Y	121.23	84.56	205.82	0.217	1.434	14.59
Al_8Fe_4La	118.10	81.19	198.17	0.220	1.454	13.90
Al_8Fe_4Ce	116.68	81.01	197.36	0.218	1.440	14.07
Al_8Fe_4Pr	117.69	81.36	198.36	0.219	1.447	14.02
Al_8Fe_4Nd	118.52	81.93	199.76	0.219	1.447	14.09
Al_8Fe_4Pm	119.51	82.76	201.72	0.218	1.444	14.23
Al_8Fe_4Sm	119.99	83.12	202.59	0.219	1.444	14.28
Al_8Fe_4Eu	120.49	83.61	203.70	0.218	1.441	14.37
Al_8Fe_4Gd	120.63	83.96	204.44	0.218	1.437	14.48
Al_8Fe_4Tb	121.16	84.28	205.26	0.218	1.438	14.50
Al_8Fe_4Dy	121.41	84.65	206.05	0.217	1.434	14.69
Al_8Fe_4Ho	121.83	84.94	206.78	0.217	1.434	14.63
Al_8Fe_4Er	122.25	85.24	207.50	0.217	1.434	14.67
Al_8Fe_4Tm	122.78	85.25	207.68	0.218	1.440	14.58
Al_8Fe_4Yb	112.76	77.80	189.76	0.220	1.449	13.55
Al_8Fe_4Lu	117.26	81.02	197.57	0.219	1.447	13.97

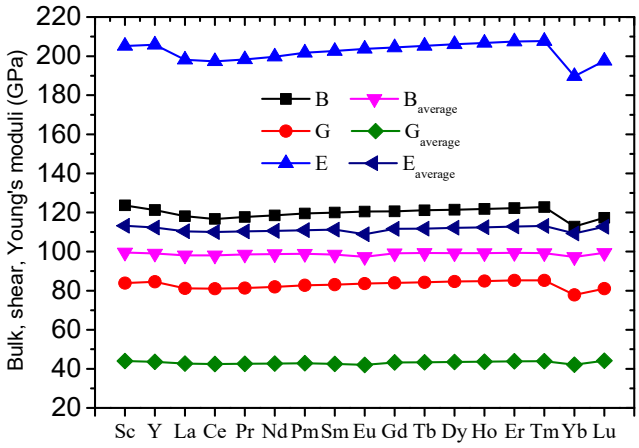

Figure 1. The calculated bulk, shear, and Young's modulus of Al_8Fe_4RE IMCs.

In order to illustrate the elastic anisotropy of Al_8Fe_4RE IMCs, the surfaces of Young's modulus for Al_8Fe_4RE IMCs are shown in Figure 2. The three-dimensional surface exhibited a spherical shape for an isotropic crystal. As can be seen in Figure 2, the isosurfaces of Young's modulus exhibited remarkable anisotropic behavior for all the Al_8Fe_4RE IMCs. In the light of the Pugh criterion [43], the B/G ratios for the 17 Al_8Fe_4RE IMCs were all smaller than 1.75, which reveals that the IMCs are prone to brittleness. A theoretical model [44] of linking Vickers hardness and moduli is via $Hv = 2 \times (k^{-2}G)^{0.585} - 3$, where Hv is Vickers hardness and k is the ratio B/G. The calculated Vickers hardness of the 17 Al_8Fe_4RE IMCs were all about 14 GPa.

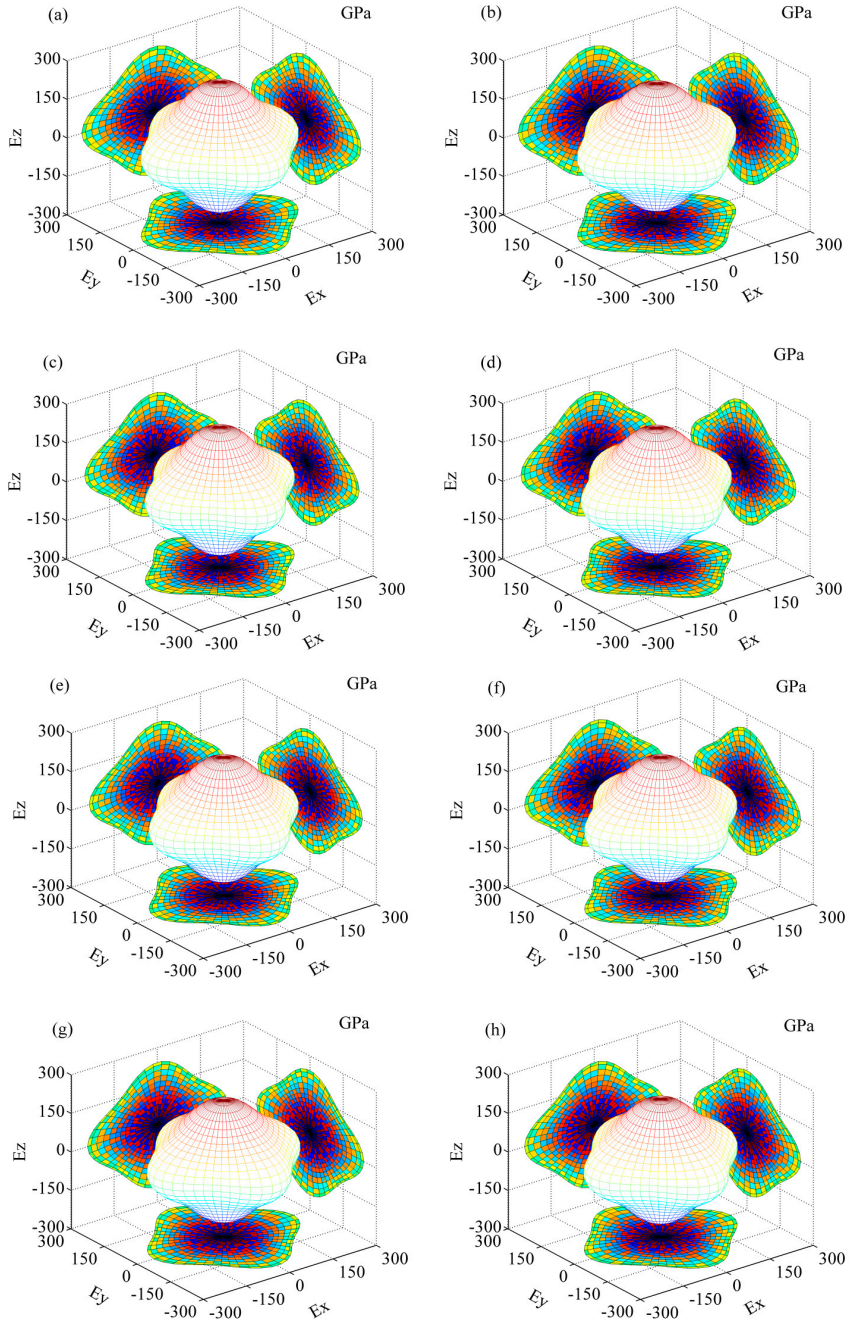

Figure 2. *Cont.*

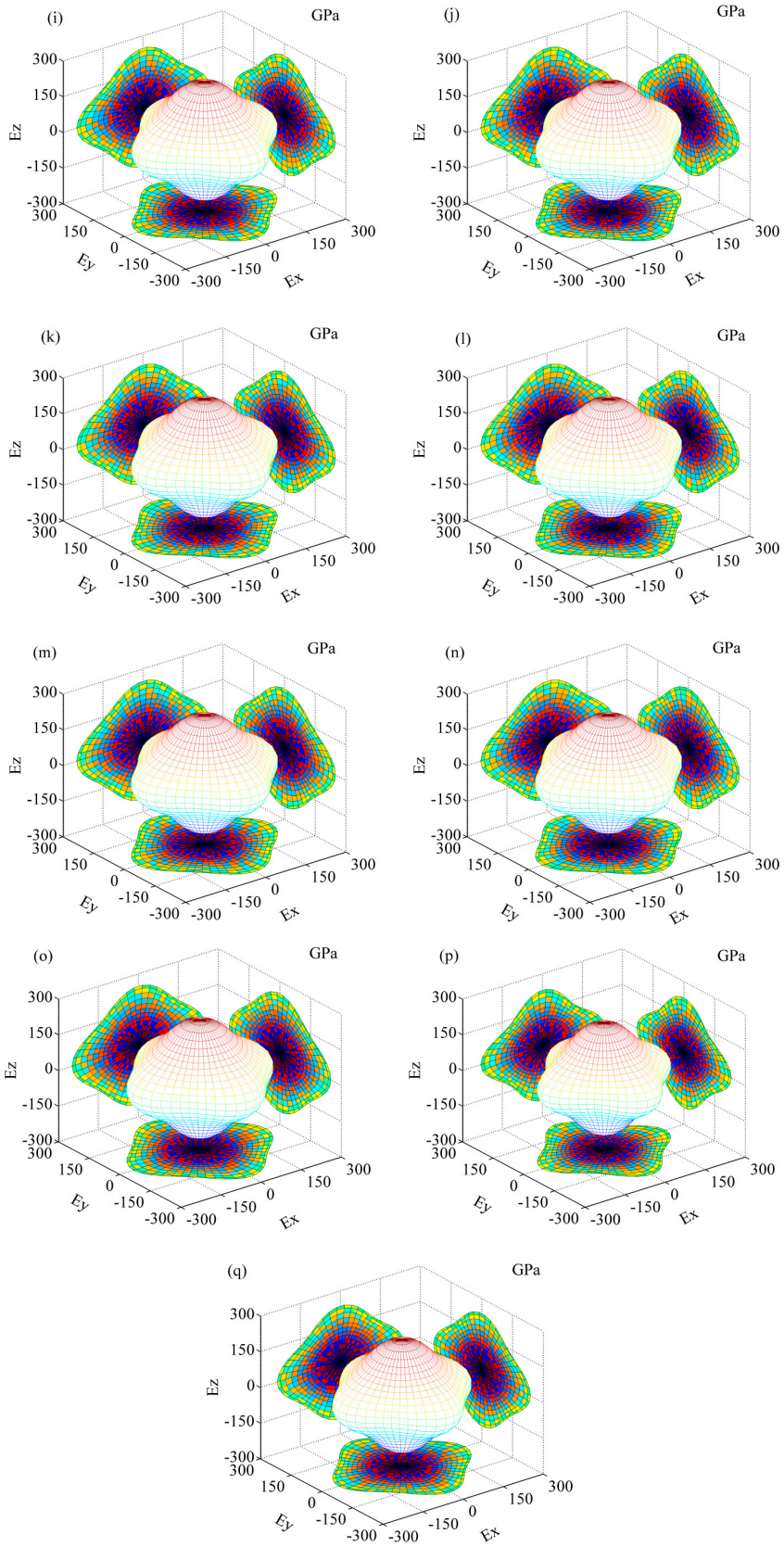

Figure 2. The 3D curved surface of the Young's modulus of Al_8Fe_4RE IMCs. (**a**) Al_8Fe_4Sc; (**b**) Al_8Fe_4Y; (**c**) Al_8Fe_4La; (**d**) Al_8Fe_4Ce; (**e**) Al_8Fe_4Pr; (**f**) Al_8Fe_4Nd; (**g**) Al_8Fe_4Pm; (**h**) Al_8Fe_4Sm; (**i**) Al_8Fe_4Eu; (**j**) Al_8Fe_4Gd; (**k**) Al_8Fe_4Tb; (**l**) Al_8Fe_4Dy; (**m**) Al_8Fe_4Ho; (**n**) Al_8Fe_4Er; (**o**) Al_8Fe_4Tm; (**p**) Al_8Fe_4Yb; (**q**) Al_8Fe_4Lu.

3.3. Electronic Properties

The density of states (DOS), electron localization function (ELF), and bonding charge density (BCD) for Al_8Fe_4Sc are plotted in Figure 3 as an example. It can be seen from Figure 3 that Al_8Fe_4Sc showed metallic behavior, and the DOS at the Fermi level was mainly dominated by the Fe-3d state and Sc-3d states, evidencing the hybridization at the Fermi level. The ELF and BCD showed a depletion of the electronic density (ED) at the Al and Sc lattice sites, along with an increment of the ED at the Fe sites. This feature is consistent with the DOS plots in Figure 3a, demonstrating the hybridization of Fe-3d and Sc-3d. For the other Al_8Fe_4RE IMCs, their electronic structures were all similar to Al_8Fe_4Sc, so they are not shown here (see Supplementary data).

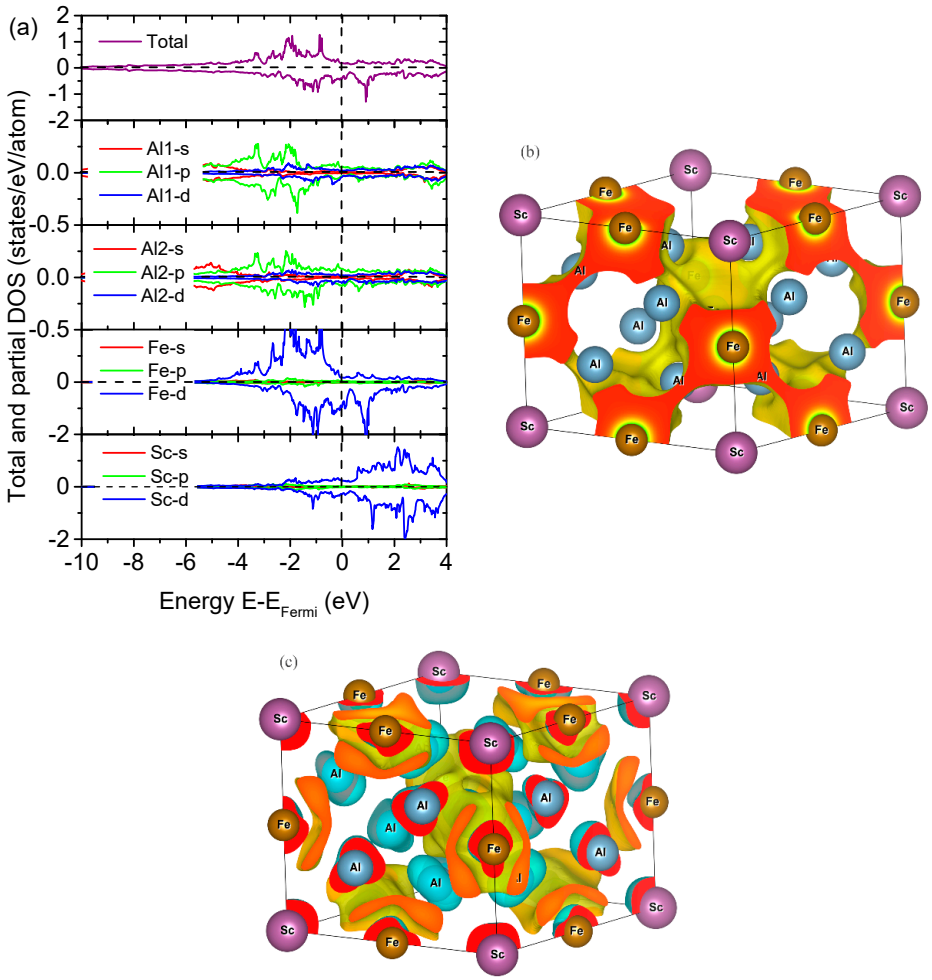

Figure 3. (**a**) The total and partial density of states, (**b**) electron localization function, and (**c**) bonding charge density of Al_8Fe_4Sc.

3.4. Lattice Dynamical Properties

In order to check the dynamic stability, the phonon dispersion (PD) curves of Al_8Fe_4RE IMCs were calculated by combing VASP and PHONOPY codes [45]. For the PD calculation, we used $2 \times 2 \times 2$ supercell containing 104 atoms for Al_8Fe_4RE and $5 \times 5 \times 5$ k-point mesh. The calculated PD curves along Z-Γ-X-P-N-Γ directions and the phonon density of states (PDOS) are plotted in Figure 4. Among the 17 Al_8Fe_4RE IMCs, only Al_8Fe_4Y had the imaginary frequency, indicating that Al_8Fe_4Y is dynamically unstable. For the others, the calculated PD curves did not have any soft mode, confirming the dynamic stability of Al_8Fe_4RE (RE, La–Lu) IMCs. The heat capacity C_v and entropy S of Al_8Fe_4RE IMCs are shown in Figure 5. The calculated C_v exhibited the expected T^3 power law

in the low temperature, and C_v reached a classic limit of 324.246 J·(K·mol)$^{-1}$ at high temperature, which is consistent with the classic law of Dulong–Petit. However, no experimental data of C_v of Al_8Fe_4RE could be found in the literatures. The present calculations should be a prediction, and further experiments are needed in the future.

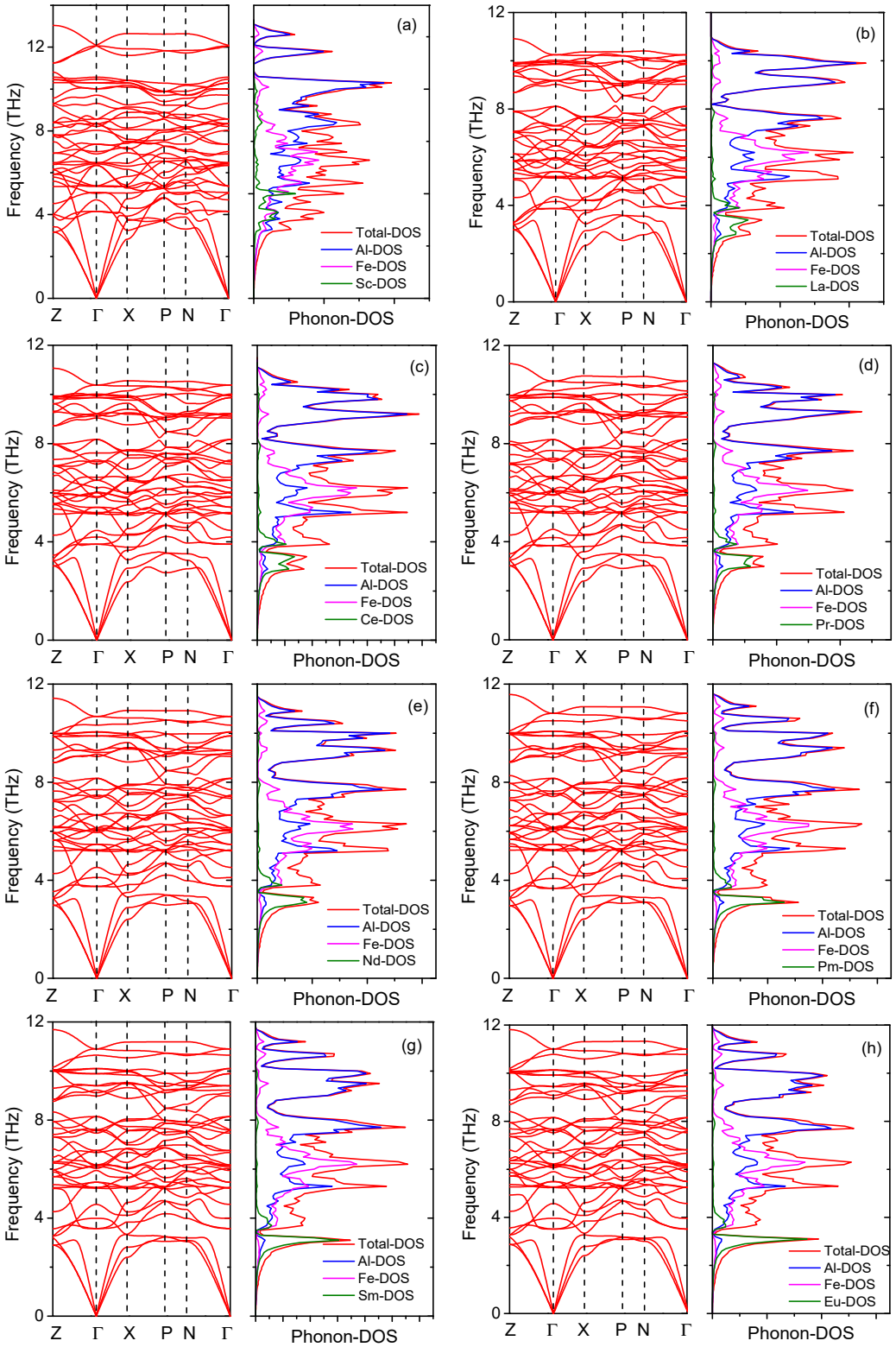

Figure 4. *Cont.*

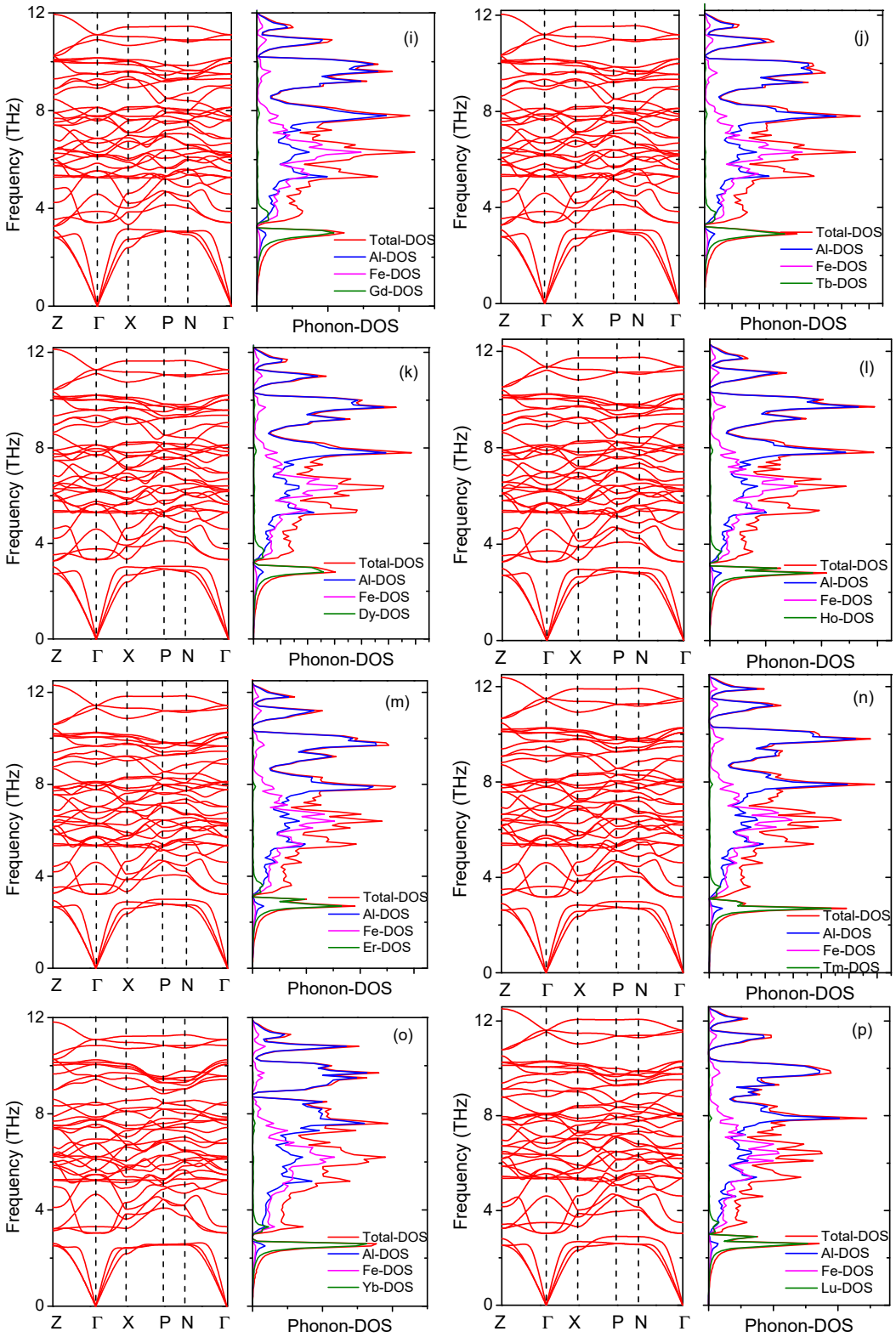

Figure 4. Phonon dispersion spectrum and phonon density of state for Al_8Fe_4RE(RE = Sc, La–Lu) IMCs. (**a**) Al_8Fe_4Sc; (**b**) Al_8Fe_4La; (**c**) Al_8Fe_4Ce; (**d**) Al_8Fe_4Pr; (**e**) Al_8Fe_4Nd; (**f**) Al_8Fe_4Pm; (**g**) Al_8Fe_4Sm; (**h**) Al_8Fe_4Eu; (**i**) Al_8Fe_4Gd; (**j**) Al_8Fe_4Tb; (**k**) Al_8Fe_4Dy; (**l**) Al_8Fe_4Ho; (**m**) Al_8Fe_4Er; (**n**) Al_8Fe_4Tm; (**o**) Al_8Fe_4Yb; (**p**) Al_8Fe_4Lu.

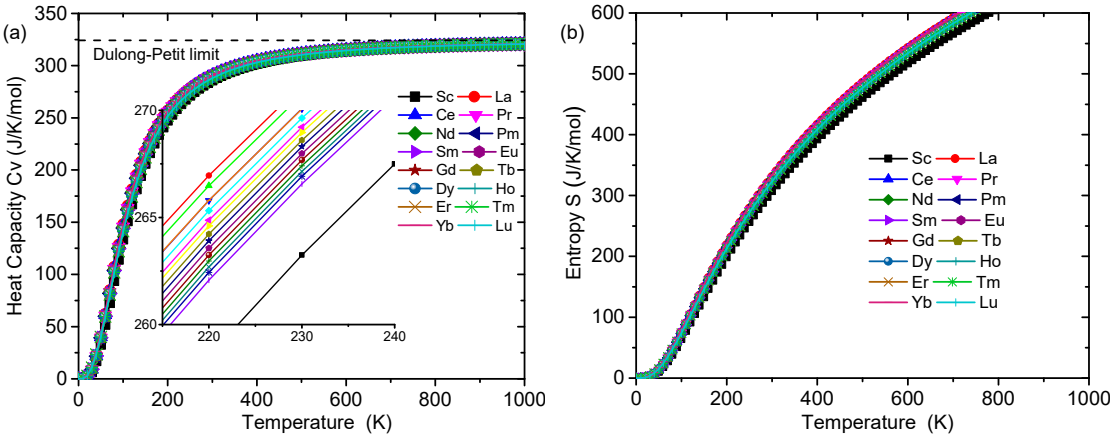

Figure 5. The (**a**) heat capacity and (**b**) entropy of Al_8Fe_4RE (RE = Sc, La–Lu) IMCs.

4. Summary

Using the first-principle calculations, the phase stability, elastic constants, various moduli, hardness, electronic, and lattice dynamical properties of Al_8Fe_4RE IMCs were investigated. The calculated lattice constants were all consistent with the experimental data. The formation enthalpies were all negative, meaning all the IMCs are stable from a thermodynamic point view. The calculated Young's and shear modulus were three times as large as that of Al and two times as large as that of arithmetic average values. The values of hardness of Al_8Fe_4RE IMCs were all about 14 GPa. All of abovementioned mechanical properties indicate that Al_8Fe_4RE IMCs may be a good strengthening phase for Al–Fe-based alloys. The calculated PD of Al_8Fe_4Y had a soft mode, and the others had no soft mode at any vectors, which means that Al_8Fe_4Y is dynamically unstable, while the others are all dynamically stable. The results are beneficial for the extensive application of Al_8Fe_4RE IMCs.

Supplementary Materials: The following are available online at http://www.mdpi.com/1996-1944/12/5/701/s1, Figure S1: The total and partial density of state of Al_8Fe_4RE. (**a**) Al_8Fe_4Sc; (**b**) Al_8Fe_4Y; (**c**) Al_8Fe_4La; (**d**) Al_8Fe_4Ce; (**e**) Al_8Fe_4Pr; (**f**) Al_8Fe_4Nd; (**g**) Al_8Fe_4Pm; (**h**) Al_8Fe_4Sm; (**i**) Al_8Fe_4Eu; (**j**) Al_8Fe_4Gd; (**k**) Al_8Fe_4Tb; (**l**) Al_8Fe_4Dy; (**m**) Al_8Fe_4Ho; (**n**) Al_8Fe_4Er; (**o**) Al_8Fe_4Tm; (**p**) Al_8Fe_4Yb; (**q**) Al_8Fe_4Lu. Figure S2: The Charge density map and differential charge density map of Al_8Fe_4RE; (**a**) Al_8Fe_4Sc; (**b**) Al_8Fe_4Y; (**c**) Al_8Fe_4La; (**d**) Al_8Fe_4Ce; (**e**) Al_8Fe_4Pr; (**f**) Al_8Fe_4Nd; (**g**) Al_8Fe_4Pm; (**h**) Al_8Fe_4Sm; (**i**) Al_8Fe_4Eu; (**j**) Al_8Fe_4Gd; (**k**) Al_8Fe_4Tb; (**l**) Al_8Fe_4Dy; (**m**) Al_8Fe_4Ho; (**n**) Al_8Fe_4Er; (**o**) Al_8Fe_4Tm; (**p**) Al_8Fe_4Yb; (**q**) Al_8Fe_4Lu.

Author Contributions: Conceptualization, R.W. and Y.O.; methodology, R.W. and X.T.; formal analysis, R.W. and H.C.; writing—original draft preparation, R.W.; writing—review and editing, X.T. and Y.O.; visualization, H.C.; project administration, Y.O.

Funding: This work is financially supported by the National Natural Science Foundation of China (11464001, 51531009, 51661003), and supported by Guangxi Key Laboratory of Processing for Non-ferrous Metallic and Featured Materials (GXKFJ16-13).

Conflicts of Interest: The authors declare no conflict of interest.

References

1. Sasaki, T.T.; Ohkubo, T.; Hono, K. Microstructure and mechanical properties of bulk nanocrystalline Al–Fe alloy processed by mechanical alloying and spark plasma sintering. *Acta Mater.* **2019**, *57*, 3529–3538. [CrossRef]
2. D'Angelo, L.; D'Onofrio, L.; Gonzalez, G. Nanophase intermetallic FeAl obtained by sintering after mechanical alloying. *J. Alloy. Compd.* **2009**, *483*, 154–158. [CrossRef]
3. Wu, H.; Baker, I.; Liu, Y.; Wu, X.; Cheng, J. Magnetically-triggered heating of Fe–Al powders. *Intermetallics* **2011**, *19*, 1517–1525. [CrossRef]
4. Zienert, T.; Fabrichnaya, O. Experimental investigation and thermodynamic assessment of the Al-Fe system. *J. Alloy. Compd.* **2018**, *743*, 795–811. [CrossRef]

5. Du, Y.; Schuster, J.C.; Liu, Z.K.; Hu, R.X.; Nash, P.; Sun, W.H.; Zhang, W.W.; Wang, J.; Zhang, L.J.; Tang, C.Y.; et al. A thermodynamic description of the Al–Fe–Si system over the whole composition and temperature ranges via a hybrid approach of CALPHAD and key experiments. *Intermetallics* **2008**, *16*, 554–570. [CrossRef]
6. Hadef, F. Solid-state reactions during mechanical alloying of ternary Fe–Al–X (X = Ni, Mn, Cu, Ti, Cr, B, Si) systems: A review. *J. Magn. Magn. Mater.* **2016**, *419*, 105–118. [CrossRef]
7. Li, G.H.; Bian, X.F.; Song, K.K.; Guo, J.; Li, X.L.; Wang, C.D. Effect of Si addition on glass forming ability and thermal stability of Al–Fe–La alloys. *J. Alloy. Compd.* **2009**, *471*, L47–L50. [CrossRef]
8. Wang, X.; Guan, R.G.; Misra, R.D.K.; Wang, Y.; Li, H.C.; Shang, Y.Q. The mechanistic contribution of nanosized Al_3Fe phase on the mechanical properties of Al-Fe alloy. *Mater. Sci. Eng. A* **2018**, *724*, 452–460. [CrossRef]
9. Feng, H.; Zhang, M.; Chen, H.M.; Liang, J.L.; Tao, X.M.; Ouyang, Y.F.; Du, Y. Experimental investigation on phase equilibria in the Al–Fe–Y system at 773 K. *J. Phase Equilib. Diffus.* **2014**, *35*, 256–261. [CrossRef]
10. Zheng, H.Y.; Li, Z.; Ji, L.; Yin, F.C. Investigation of the 600 °C isothermal section of the Fe–Al–Ce ternary system. *Int. J. Mater. Res.* **2017**, *108*, 36–44. [CrossRef]
11. Feng, H.; Chen, H.M.; Ouyang, Y.F.; Tao, X.M.; Liang, J.L.; Du, Y. Experimental investigation of the Al–Fe–Nd system at 773 K. *J. Phase Equilib. Diffus.* **2014**, *35*, 86–92. [CrossRef]
12. Feng, H.; Guo, H.; Tao, X.M.; Chen, H.M.; Ouyang, Y.F.; Du, Y.; He, Y.H. Experimental investigation of the Al–Fe–Gd system at 773 K. *J. Phase Equilib. Diffus.* **2013**, *34*, 116–121. [CrossRef]
13. Jemmali, M.; Walha, S.; Pasturel, M.; Tougait, O.; Ben Hassen, R.; Noel, H. Isothermal section of the Er–Fe–Al ternary system at 800 °C. *J. Alloy. Compd.* **2010**, *489*, 421–423. [CrossRef]
14. Felner, I.; Nowik, I. Crystal structure magnetic properties and hyperfine interactions in RFe_4Al_8 (R = rare earth) system. *J. Phys. Chem. Solids* **1978**, *39*, 951–956. [CrossRef]
15. Qu, H.; Liu, W.D.; Liu, Y.Y. Analysis of the valence electron structures of the strengthening phases Al_8Fe_4Ce and Al_4Ce in Al-Fe-Ce alloy. *Adv. Mater. Res.* **2011**, *194–196*, 1291–1295. [CrossRef]
16. Shcherba, I.D.; Koterlyn, M.D.; Kushnir, A.P.; Kutjanskyj, R.R.; Synjushko, V.G.; Tsybukh, Y.D.; Yatsyk, B.M.; Margolych, I.I. Peculiarities of the valence state of Ce and Yb in RM_4Al_8 (R = rare earth; M = Cr, Mn, Fe, Cu). *J. Magn. Magn. Mater.* **1996**, *157*, 688–689. [CrossRef]
17. Gaczynski, P.; Vagizov, F.G.; Suski, W.; Kotur, B.; Wochowski, K.; Drulis, H. Magnetic properties and Mossbauer effect studies of $Ce_{1-x}Sc_xFe_4Al_8$ system. *J. Magn. Magn. Mater.* **2000**, *214*, 37–43. [CrossRef]
18. Suski, W.; Wochowski, K.; Kotur, B.Y. Magnetic and electrical properties of $Yb_{1-x}Sc_xFe_4Al_8$ alloys. *Czech. J. Phys.* **2002**, *52*, A189–A192. [CrossRef]
19. Suski, W.; Kotur, B.Y.; Wochowski, K. Magnetic and electrical properties of $Ce_{1-x}Sc_xFe_4Al_8$ system. *Phys. B* **2000**, *281*, 81–82. [CrossRef]
20. Duong, P.; Brück, E.; de Boer, F.R.; Buschow, K.H.J. Magnetic properties of $GdFe_4Al_8$ and related compounds. *Phys. B* **2001**, *294–295*, 212–216. [CrossRef]
21. Bodak, O.; Tokaychuk, Y.; Manyako, M.; Pacheco, V.; Cerny, R.; Yvon, K. Structural and magnetic properties of iron-rich compounds in the Yb–Fe–Al system. *J. Alloy. Compd.* **2003**, *354*, L10–L15. [CrossRef]
22. Palasyuk, A.M.; Kotur, B.Y.; Bauer, E.; Michor, H.; Hischer, G. Electrical conductivity of $ThMn_{12}$- and Th_2Zn_{17}-type ternary intermetallic compounds in R–T–Al systems (R = Y, La, Ce, Gd, Tb; T = Mn, Fe). *J. Alloy. Compd.* **2004**, *367*, 205–210. [CrossRef]
23. Dmitriev, V.M.; Terekhov, A.V.; Suski, W.; Ishchenko, L.A.; Cwik, J.; Palewski, T.; Kotur, B.Y.; Talik, E. Negative magnetoresistivity of the RM_4Al_8 (R = Sc, Y, Ce, Yb, Lu; M = Cr, Mn, Fe) ternaries with the $ThMn_{12}$-type crystal structure. *J. Alloy. Compd.* **2008**, *452*, 217–224. [CrossRef]
24. Kang, Y.M.; Chen, N.X.; Shen, J. Atomistic simulation of the lattice constants and lattice vibrations in RT_4Al_8 (R = Nd, Sm; T = Cr, Mn, Cu, Fe). *J. Alloy. Compd.* **2003**, *352*, 26–33. [CrossRef]
25. Kang, Y.M.; Chen, N.X.; Shen, J. Lattice vibration of $Ce_{1-x}Sc_xFe_4Al_8$. *J. Phys. Chem. Solids* **2003**, *64*, 433–441. [CrossRef]
26. Kresse, G.; Furthmuller, J. Efficient iterative schemes for ab initio total-energy calculations using a plane-wave basis set. *Phys. Rev. B* **1996**, *54*, 11169–11186. [CrossRef]
27. Kresse, G.; Furthmuller, J. Efficiency of ab-initio total energy calculations for metals and semiconductors using a plane-wave basis set. *Comput. Mater. Sci.* **1996**, *6*, 15–50. [CrossRef]
28. Blöchl, P.E. Projector augmented-wave method. *Phys. Rev. B* **1994**, *50*, 17953–17979. [CrossRef]

29. Kresse, G.; Joubert, D. From ultrasoft pseudopotentials to the projector augmented-wave method. *Phys. Rev. B* **1999**, *59*, 1758–1775. [CrossRef]
30. Perdew, J.P.; Burke, K.; Ernzerhof, M. Generalized gradient approximation made simple. *Phys. Rev. Lett.* **1996**, *77*, 3865–3868. [CrossRef] [PubMed]
31. Monkhorst, H.J.; Pack, J.D. Special points for Brillouin-zone integrations. *Phys. Rev. B* **1976**, *13*, 5188–5192. [CrossRef]
32. Methfessel, M.; Paxton, A.T. High-precision sampling for Brillouin-zone integration in metals. *Phys. Rev. B* **1989**, *40*, 3616–3621. [CrossRef]
33. Fu, C.L.; Wang, X.D.; Ye, Y.Y.; Ho, K.M. Phase stability, bonding mechanism, and elastic constants of Mo_5Si_3 by first-principles calculation. *Intermetallics* **1999**, *7*, 179–184. [CrossRef]
34. Voigt, W. *Lehrbuch de Kristallphysik*; Terubner: Leipzig, Germany, 1928.
35. Reuss, A.; Angew, Z. Berechnung del fliessgrenze von misch- kristallen auf grund der plastizitatbedingung for einkristalle. *Math. Mech.* **1929**, *9*, 49–58.
36. Hill, R. The elastic behaviour of a crystalline aggregate. *Proc. Phys. Soc. Lond. A* **1952**, *65*, 349–352. [CrossRef]
37. Tao, X.M.; Jund, P.; Colinet, C.; Tedenac, J.C. Phase stability and physical properties of Ta_5Si_3 compounds from first-principles calculations. *Phys. Rev. B* **2009**, *80*, 104103. [CrossRef]
38. Hackenberg, R.E.; Gao, M.C.; Kaufman, L.; Shiflet, G.J. Thermodynamics and phase equilibria of the Al–Fe–Gd metallic glass-forming system. *Acta Mater.* **2002**, *50*, 2245–2258. [CrossRef]
39. Tao, X.M.; Ouyang, Y.F.; Liu, H.S.; Zeng, F.J.; Feng, Y.P.; Jin, Z.P. Ab initio calculations of mechanical and thermodynamic properties for the B2-based AlRE. *Comput. Mater. Sci.* **2007**, *40*, 226–233. [CrossRef]
40. Tao, X.M.; Ouyang, Y.F.; Liu, H.S.; Zhong, X.P.; Feng, Y.P.; Du, Y.; Jin, Z.P. Elastic constants of B2-MgRE (RE = Sc, Y, La–Lu) calculated with first-principles. *Solid State Commun.* **2008**, *148*, 314–318. [CrossRef]
41. Tao, X.M.; Ouyang, Y.F.; Liu, H.S.; Zeng, F.J.; Feng, Y.P.; Du, Y.; Jin, Z.P. Ab initio calculation of the total energy and elastic properties of Laves phase C15 Al_2RE (RE = Sc, Y, La, Ce–Lu). *Comput. Mater. Sci.* **2008**, *44*, 392–399. [CrossRef]
42. Seitz, F.; Turnbull, D. *Solid State Physics: Advance in Research and Applications*; Academic Press: New York, NY, USA; London, UK, 1964; Volume 16.
43. Pugh, S.F. Relations between the elastic moduli and the plastic properties of polycrystalline pure metals. *Philos. Mag.* **1954**, *45*, 823–843. [CrossRef]
44. Chen, X.Q.; Niu, H.Y.; Li, D.Z.; Li, Y.Y. Modeling hardness of polycrystalline materials and bulk metallic glasses. *Intermetallics* **2011**, *19*, 1275–1281. [CrossRef]
45. Togo, A.; Oba, F.; Tanaka, I. First-principles calculations of the ferroelastic transition between rutile-type and $CaCl_2$-type SiO_2 at high pressures. *Phys. Rev. B* **2008**, *78*, 134106. [CrossRef]